Available online at www.sciencedirect.com

ScienceDirect

Geochimica et Cosmochimica Acta 172 (2016) 127–138

Geochimica et Cosmochimica Acta

www.elsevier.com/locate/gca

Quantifying uncertainty of past pCO_2 determined from changes in C_3 plant carbon isotope fractionation

Ying Cui *, Brian A. Schubert

School of Geosciences, University of Louisiana at Lafayette, Lafayette, LA 70504, United States

Received 25 June 2015; accepted in revised form 26 September 2015; Available online 9 October 2015

Abstract

Knowledge of the past concentrations of atmospheric CO_2 level (pCO_2) is critical to understanding climate sensitivity to changing pCO_2. Towards this, a new proxy for pCO_2 has been developed based on changes in carbon isotope fractionation ($\Delta^{13}C$) in C_3 land plants. The accuracy of this approach has been validated against ice-core pCO_2 records, suggesting the potential to apply this proxy to other geological periods; however, no thorough uncertainty assessment of the proxy has been conducted. Here, we first analyze the uncertainty in the model-curve fit through the experimental data using a bootstrap approach. Then, errors of the five input parameters for the proxy are evaluated using sensitivity analysis; these include the carbon isotope composition of atmospheric CO_2 ($\delta^{13}C_{CO2}$) and that of the plant material ($\delta^{13}C_{org}$) for two time periods, a reference time ($t = 0$) and the time period of interest (t), and the value of pCO_2 at time $t = 0$. We then propagated the errors on the reconstructed pCO_2 using a Monte Carlo random sampling approach that combined the uncertainties of the curve fitting and the five inputs for a scenario in which the reference time was the Holocene with a target period for the reconstructed pCO_2 during the Cenozoic. We find that the error in the reconstructed $pCO_{2(t)}$ increases with increasing $pCO_{2(t)}$, yet remains <122% (positive error) and <40% (negative error) for $pCO_{2(t)} < 1000$ ppmv. The error assessment suggests that it can be used with confidence for much of the Cenozoic and perhaps the majority of the last 400 million years, which is characterized by pCO_2 levels generally less than 1000 ppmv. Towards this, an application of this uncertainty analysis is presented for the Paleogene (52–63 Ma) using published data. The resulting $pCO_{2(t)}$ levels calculated using this method average 470 +288/−147 ppmv (1σ, $n = 75$), and overlap with previous $pCO_{2(t)}$ estimates determined for this time period using stomata, liverwort, and paleosol proxies. The analysis presented here assumes that the paleoenvironment in which the plants grew is unknown and is determined to be the largest source of error in the reconstructed $pCO_{2(t)}$ levels; errors in $pCO_{2(t)}$ could be reduced provided independent determination of the paleoenvironmental conditions at the fossil site.

1. INTRODUCTION

Various methods have been employed for the reconstruction of ancient atmospheric carbon dioxide levels (pCO_2) using terrestrial substrates [paleosol carbonate (Cerling, 1991; Ekart et al., 1999; Breecker et al., 2010), plant stomatal index (Royer et al., 2001; Beerling et al., 2009), liverworts (Fletcher et al., 2005; Fletcher et al., 2006; Fletcher et al., 2008), sodium carbonate equilibrium (Lowenstein and Demicco, 2006), leaf gas exchange model (Konrad et al., 2008; Franks et al., 2014), weathering profiles (Kanzaki and Murakami, 2015), C_3 terrestrial plants (Schubert and Jahren, 2013, 2015)] and marine substrates [phytoplankton (Pagani et al., 1999; Freeman and Pagani, 2005; Hoins et al., 2015), boron isotope ratios (Pearson and Palmer, 2000; Pearson et al., 2009), changes in seawater chemistry (Demicco et al., 2003), boron/calcium ratios (Tripati et al., 2009), inverse modeling of benthic oxygen

* Corresponding author.
E-mail address: yxc3845@louisiana.edu (Y. Cui).

http://dx.doi.org/10.1016/j.gca.2015.09.032
0016-7037/

isotope records (van de Wal et al., 2011)]. Although sizable scatter in reconstructed pCO_2 exists, especially for intervals of higher pCO_2 (Beerling and Royer, 2011), efforts to improve the accuracy and precision of the pCO_2 estimates (e.g., Demicco et al., 2003; Breecker et al., 2010; Royer, 2014) have led to greater agreement among the diverse techniques. Each proxy has its advantages and disadvantages with respect to the temporal resolution (long-term trends *versus* short-term excursions), applicable time intervals (anthropogenic period, glacial-interglacial cycles, Cenozoic, and Phanerozoic, etc.), and sensitivity across a range of pCO_2 levels (see Royer et al., 2001). Beyond the suitability of each proxy for reconstructing pCO_2 across the time period of interest, recognition for the need to better quantify the precision in individual pCO_2 estimates has led to rigorous statistical analyses (i.e., Monte Carlo error assessment) of the propagation of uncertainty for several of the pCO_2 proxies [e.g., stomatal index, Beerling et al. (2009); paleosol carbonate, Breecker (2013); leaf gas exchange model, Franks et al. (2014); phytoplankton, Freeman and Pagani (2005); liverworts, Fletcher et al. (2008); boron isotopes (Martínez-Botí et al., 2015)]. The C_3 plant carbon isotope fractionation based pCO_2 proxy is a novel approach, which has been developed based on the effect of pCO_2 on carbon isotope fractionation during photosynthesis (Schubert and Jahren, 2012). This relationship has been applied to reconstruct the pCO_2 across the Pleistocene-Holocene transition (Schubert and Jahren, 2015) and the Paleocene-Eocene Thermal Maximum (Schubert and Jahren, 2013), and to interpret changes in speleothem $\delta^{13}C$ values (Wong and Breecker, 2015). However, no quantitative error assessment has been conducted to evaluate the uncertainty of the reconstructed pCO_2. Here we assess the error associated with this proxy. We first consider the uncertainty of the curve fitting. We then produce a fully propagated assessment of error using a Monte Carlo random sampling approach in order to quantify the uncertainty in this proxy across a wide range of pCO_2 (i.e., ~110 to ~2000 ppmv) and compare the errors in this new proxy to other published proxies. We also conduct sensitivity analyses on the uncertainty associated with each input parameter individually.

2. METHODS

2.1. Curve fitting

Experiments growing plants in controlled chambers across multiple levels of pCO_2 up to 4200 ppmv revealed a hyperbolic relationship between net carbon isotope fractionation $[\Delta^{13}C = (\delta^{13}C_{CO2} - \delta^{13}C_{org})/(1 + \delta^{13}C_{org}/1000)]$ and pCO_2 (Schubert and Jahren, 2012), where $\delta^{13}C_{CO2}$ and $\delta^{13}C_{org}$ represent the carbon isotope value of atmospheric CO_2 and plant tissue, respectively. These data, combined with literature data, showed that the change in $\Delta^{13}C$ value per ppmv of pCO_2 (i.e., S, ‰/ppmv) is consistent across a wide range of species growing in diverse conditions according to the following equation (Schubert and Jahren, 2012) (Fig. 1):

$$S = (A^2)(B)/[A + (B)(pCO_2 + C)]^2 \quad (1)$$

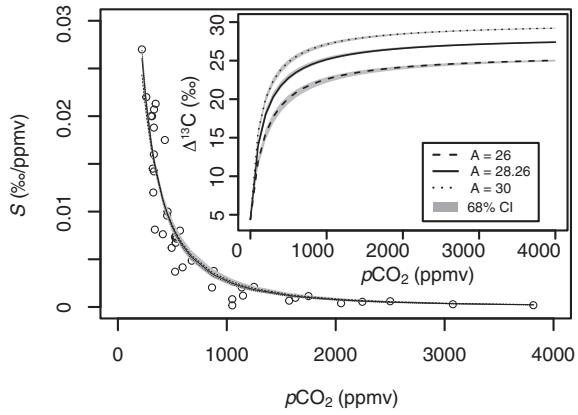

Fig. 1. The effect of pCO_2 on C_3 land plant carbon isotope fractionation based on field and chamber experiments on a wide range of C_3 land plant species. The amount of carbon isotope fractionation per change in pCO_2 (S, ‰/ppmv) as a function of pCO_2 (Eq. (1)) is plotted for three choices of A (A = 26, 28.26, and 30; calculated values for B and C, for each A, are provided in Table 1). Note the similarity among the three S-curves. Circles are plotted as the midpoint of the range of pCO_2 tested for each study. All data and references are provided in Table DR2 within Schubert and Jahren (2015). Inset: $\Delta^{13}C$ value plotted as a function of pCO_2 (Eq. (2)) with the same values for A, B, and C (Table 1). The shaded regions represent the 68% confidence interval based on 10,000 bootstrap iterations.

where A, B and C are curve fitting parameters, discussed below. The integration of Eq. (1) yields a generalized hyperbolic relationship between $\Delta^{13}C$ and pCO_2 (Eq. (2)):

$$\Delta^{13}C = [(A)(B)(pCO_2 + C)]/[A + (B)(pCO_2 + C)] \quad (2)$$

The classic equation modeling carbon isotope fractionation between plants and the atmosphere (Farquhar et al., 1989) states that:

$$\Delta^{13}C = a + (b - a)(c_i/c_a) \quad (3)$$

where a and b are constants representing the isotopic fractionation due to diffusion through the plant's stomata and subsequent catalysis by Ribulose-1,5-biphosphate carboxylase/oxygenase (RuBisCO), respectively; and c_i/c_a is the ratio of intercellular and ambient partial pressures of CO_2. The value for a is set to 4.4‰ (Craig, 1953; Cerling et al., 1991) and values for b range in the literature from 26‰ to 30‰ (Christeller et al., 1976; Wong et al., 1979; Farquhar et al., 1982; Roeske and O'Leary, 1984; Guy et al., 1993; Lloyd and Farquhar, 1994; Suits et al., 2005) and Schubert and Jahren (2012, 2013, 2015) used a value of 28.26‰ based on data from their elevated pCO_2 experiments. Because c_i/c_a must be between 0 and 1, Eq. (3) constrains the maximum and minimum values for $\Delta^{13}C$ where: (1) $\Delta^{13}C = a$ at $c_i/c_a = 0$ (i.e., $\Delta^{13}C = 4.4‰$ at $pCO_2 = 0$ ppmv) and (2) $\Delta^{13}C = b$ when $c_i/c_a = 1$ (i.e., $\Delta^{13}C$ cannot exceed b). We note that this maximum fractionation value, b, in Eq. (3) is equivalent to the asymptote, A, in Eq. (2). Values for B and C were determined iteratively by minimizing the root mean square error (RMSE) between the observed data and the fitted curve (Eq. (1)) across the full range of reported values

Table 1
B and C values calculated across the full range of potential A values.

A	B	C	RMSE
26	0.16	32.88	0.002732
27	0.19	28.40	0.002672
28	0.21	24.70	0.002633
28.26[a]	0.22	23.85	0.002625
29	0.24	21.68	0.002607
30	0.27	19.20	0.002591

[a] A = 28.26 is the value reported within Schubert and Jahren (2012) and used in their previous pCO_2 reconstructions (Schubert and Jahren 2013, 2015). The lowest RMSE results from A = 30.

for b (i.e., A) = 26–30‰, subject to these two constraints, using the "Solver" add-in within Excel (Table 1).

In order to assess the uncertainty in the curve fitting (Fig. 1) and calculate a statistically robust confidence interval, we performed a bootstrap on the residual between the curve fitting and the data following the methods described in Efron and Tibshirani (1994). We calculated the residual, i.e. the differences between the 40 observed data points and the best-fit curve, using three A values (A = 26, 28.26, and 30), which span the full range of reported values. We then performed a random sampling of the residuals ($n = 40$) with replacement for each A value, assuming equal probability of each residual. The newly sampled residual was then added back to the original fitted curve to create a pseudo dataset. A new curve fitting with the best-fit B and C values was determined using the pseudo dataset by minimizing the RMSE while maintaining the two constraints described above. The minimization of RMSE for the non-linear curve with constraints was realized in R (R Core Team, 2015) using function "solnp" in the "Rsolnp" package (Ye, 1987). This process was repeated 10,000 times to generate 10,000 values of B and the corresponding C values. The confidence interval of B was constructed by specifying the 16th and 84th percentile of all the bootstrapped B values. The R code, which includes instructions on how to use it for the bootstrap analysis, is provided in Supplementary Material.

2.2. Quantifying paleo-pCO_2

Because the $\Delta^{13}C$ value of modern C_3 plant tissue shows high variability (e.g., Diefendorf et al., 2010; Matson et al., 2012), even among plants growing under the same environmental conditions (e.g., Leavitt and Newberry, 1992; Flanagan et al., 1997; Bonal et al., 2000), and within highly managed arboretums and botanical gardens (Jahren, 2004), Eq. (2) cannot be used directly to calculate pCO_2 (Schubert and Jahren, 2012). Instead, the terrestrial C_3 plant organic-carbon isotope pCO_2 proxy works by examining relative changes in the $\Delta^{13}C$ value between the time of interest ($\Delta^{13}C_{(t)}$) and the $\Delta^{13}C$ value at a chosen initial time ($\Delta^{13}C_{(t=0)}$), designated within Schubert and Jahren (2015) as "$\Delta(\Delta^{13}C)$" where:

$$\Delta(\Delta^{13}C) = \Delta^{13}C_{(t)} - \Delta^{13}C_{(t=0)} \quad (4)$$

which can be expanded as:

$$\Delta(\Delta^{13}C) = \frac{(\delta^{13}C_{CO_2(t)} - \delta^{13}C_{org(t)})}{(1 + \delta^{13}C_{org(t)}/1000)} - \frac{(\delta^{13}C_{CO_2(t=0)} - \delta^{13}C_{org(t=0)})}{(1 + \delta^{13}C_{org(t=0)}/1000)} \quad (5)$$

We can also rewrite Eq. (2) in terms of a relative change in $\Delta^{13}C$ value [i.e., $\Delta(\Delta^{13}C)$] resulting from a change in pCO_2:

$$\Delta(\Delta^{13}C) = \frac{[(A)(B)(pCO_{2(t)} + C)]}{[A + (B)(pCO_{2(t)} + C)]} - \frac{[(A)(B)(pCO_{2(t=0)} + C)]}{[A + (B)(pCO_{2(t=0)} + C)]} \quad (6)$$

Then, by rearranging Eq. (6), one can solve for pCO_2 at any time t ($pCO_{2(t)}$):

$$pCO_{2(t)} = \frac{\Delta(\Delta^{13}C)\cdot A^2 + \Delta(\Delta^{13}C)\cdot A\cdot B\cdot pCO_{2(t=0)} + 2\cdot\Delta(\Delta^{13}C)\cdot A\cdot B\cdot C + \Delta(\Delta^{13}C)\cdot B^2\cdot C\cdot pCO_{2(t=0)} + \Delta(\Delta^{13}C)\cdot B^2\cdot C^2 + A^2\cdot B\cdot pCO_{2(t=0)}}{A^2\cdot B - \Delta(\Delta^{13}C)\cdot A\cdot B - \Delta(\Delta^{13}C)\cdot B^2\cdot pCO_{2(t=0)} - \Delta(\Delta^{13}C)\cdot B^2\cdot C} \quad (7)$$

Within Eq. (7), values for A, B and C are the curve fitting parameters, $pCO_{2(t=0)}$ is the initial pCO_2 level (known), and $\Delta(\Delta^{13}C)$ is calculated using Eq. (5).

2.3. Monte Carlo error assessment

We used R to perform Monte Carlo error propagation through Eq. (7) for $pCO_{2(t)} = \sim 110$ to ~ 2000 ppmv. Error related to the curve fitting equation (A, B, and C within Eqs. (1) and (2)) and all the input values ($\delta^{13}C_{CO2(t)}$, $\delta^{13}C_{org(t)}$, $\delta^{13}C_{CO2(t=0)}$, $\delta^{13}C_{org(t=0)}$, $pCO_{2(t=0)}$) required for Eq. (7) were considered in the Monte Carlo error assessment. The precision for each input is reported as $\pm 1\sigma$. We note that depending on the time period of interest, values for $\delta^{13}C_{CO2(t)}$ and $\delta^{13}C_{CO2(t=0)}$ can be determined from air bubbles trapped in ice (e.g., Schmitt et al., 2012) or reconstructions based on marine carbonate $\delta^{13}C$ values (e.g., Passey et al., 2002; Strauss and Peters-Kottig, 2003; Tipple et al., 2010).

The errors of the input variables were assumed to be Gaussian distributed. Values for each input were randomly drawn from normal distributions defined by the

pre-determined means and standard deviations. 10,000 $pCO_{2(t)}$ values were calculated using 10,000 randomly generated sets of input values. The $pCO_{2(t)}$ value we report is the median of the 10,000 iterations. The 16th and 84th percentiles of the 10,000 iterations of $pCO_{2(t)}$ values were determined to construct the 68% confidence interval, similar to that in Breecker (2013), Franks et al. (2014), and Royer et al. (2014). The positive error of the reconstructed $pCO_{2(t)}$ represents the difference between the 84th percentile value and the median, and the negative error represents the difference between the 16th percentile value and the median.

3. RESULTS

3.1. Uncertainties in curve fitting parameters A, B and C

Differences among the hyperbolic and *S* curves for A = 26, 28.26, and 30 are shown in Fig. 1. Across the entire range in possible A values, the absolute $\Delta^{13}C$ value for a given pCO_2 level differs for each of the hyperbolic curves (Fig. 1, inset), but the relative changes in $\Delta^{13}C$ for a given change in pCO_2 (i.e., the slopes of each hyperbolic curve; *S*, ‰/ppmv) are nearly identical (Fig. 1). Thus, regardless of the value for A chosen, the calculated $pCO_{2(t)}$ will be similar at low to moderate $pCO_{2(t)}$ (Supplementary Fig. 1), consistent with the result shown for subambient $pCO_{2(t=0)}$ conditions (Schubert and Jahren, 2015). The $\Delta^{13}C$ value approaches an asymptote of 26 (A = 26), 28.26 (A = 28.26), and 30‰ (A = 30) for the three choices of A, and all the curves cross the *y*-axis at 4.4‰ (i.e., $\Delta^{13}C = 4.4‰$ when $pCO_2 = 0$ ppmv) (Fig. 1, inset). The 68% confidence intervals for the three *S* curves determined from the bootstrap analysis overlap, further suggesting that the choice of A plays a minor role in the reconstructed $pCO_{2(t)}$ value, especially at low $pCO_{2(t)}$. The lowest RMSE was determined to occur with A = 30, but the RMSE value was only marginally lower than with A = 28.26 (RMSE = 0.002591 *versus* 0.002625) (Table 1). Because the choice of A value within this range (A = 26–30) is somewhat subjective, we here maintain the A = 28.26 value used by Schubert and Jahren (2012, 2013, and 2015). This choice of A value could potentially improve the accuracy in the reconstructed $pCO_{2(t)}$, especially at very high $pCO_{2(t)}$, as it falls near the midpoint of reported values (Supplementary Fig. 1). The uncertainty on the reconstructed $pCO_{2(t)}$, however, will be greater with A = 28.26 than with A = 30 as a result of the higher RMSE (and greater error in B) (Table 1). The 68% confidence intervals on the hyperbolic functions for the three choices of A values (Fig. 1, inset) show the asymmetric feature of the bootstrap-determined B value, with B value slightly skewed to the left for A = 30 (B = 0.28 +0.022/−0.024) and A = 26 (B = 0.17 +0.018/−0.024), and skewed to the right for A = 28.26 (B = 0.22 +0.028/−0.014). Although these curve-fitting errors were not normally distributed, we assumed a Gaussian distribution when conducting the Monte Carlo error analysis. Therefore, we conservatively applied the highest error on B for each A value (i.e., for A = 28.26, we used B = 0.22 ± 0.028).

Fig. 2 shows the Monte Carlo determined errors in $pCO_{2(t)}$ caused by the errors in the curve fitting only, while keeping the errors for all other input terms fixed at zero. The errors increase with increasing $pCO_{2(t)}$, with the positive error increasing at a greater rate than the negative error, especially at $pCO_{2(t)} > \sim 1500$ ppmv. Despite the model relationship being well constrained (Fig. 1), the saturating nature of our proxy augments the small errors in the curve fitting, resulting in increasing error, especially for the positive error, with increasing $pCO_{2(t)}$. However, we note that the positive error across the full range of $pCO_{2(t)}$ (i.e., up to ~2000 ppmv) remains <50%, with the negative error remaining <24% (Fig. 2, bottom). For $pCO_{2(t)}$ levels common to much of the Cenozoic (i.e., <1000 ppmv), the errors are less than 15% (Fig. 2, bottom).

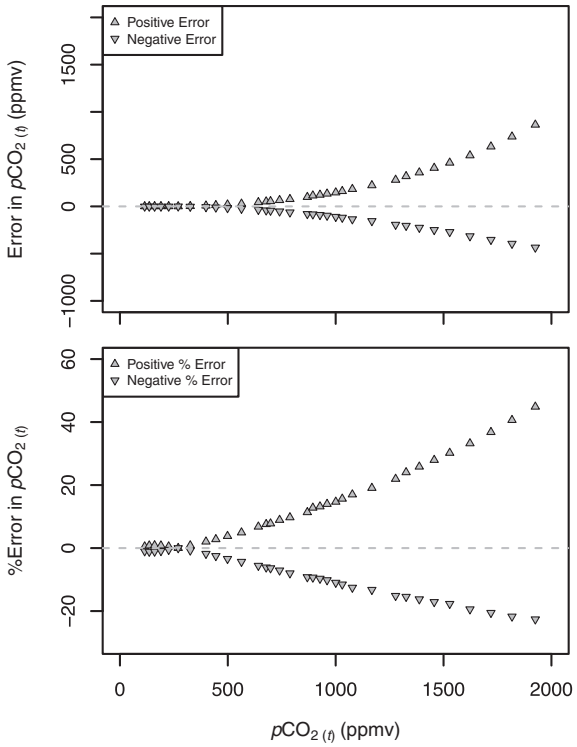

Fig. 2. The effect of uncertainty in the curve fitting (Fig. 1) on the error in $pCO_{2(t)}$ (top, ppmv; bottom, % error); all other input uncertainties were kept at 0. Error is shown for A = 28.26 with B = 0.22 ± 0.028 (±1σ). For each randomly chosen B value, corresponding values for C were calculated by solving Eq. (2) with $pCO_2 = 0$ and $\Delta^{13}C = 4.4$, such that $C = [4.4 \times (A)]/[(A - 4.4) \times (B)]$.

3.2. Full error propagation

We conducted a full Monte Carlo error propagation using the uncertainties listed in Table 2. The errors in the input parameters represent the precision associated with a scenario in which Holocene data are used for the reference period ($t = 0$) and Cenozoic data are used for time *t*. Fig. 3 shows the result of this full error propagation using the curve fitting uncertainty (Section 3.1) and the uncertainties associated with the other inputs to Eq. (7) (Table 2; see discussion below) across a wide range of reconstructed $pCO_{2(t)}$ (~110 to ~2000 ppmv). As expected, the error in $pCO_{2(t)}$

Table 2
The uncertainty of each input variable used to calculate the propagated error of $pCO_{2(t)}$ where the reference period ($t = 0$) is the Holocene ($pCO_{2(t=0)} = 270$ ppmv).

Input variable (Eq. (7))	Input values	Source	Uncertainty ($\pm1\sigma$)	Source
$pCO_{2(t\ =\ 0)}$	270 ppmv	Kawamura et al. (2007)	7 ppmv	Kawamura et al. (2007)
$\delta^{13}C_{CO2(t=0)}$	−6.4‰	Schubert and Jahren (2015)	0.1‰	Schmitt et al. (2012)
$\delta^{13}C_{CO2(t)}$	Variable[a]	Tipple et al. (2010)[a]	0.5‰	Tipple et al. (2010)
$\delta^{13}C_{org(t\ =\ 0)}$	−25.1‰	Schubert and Jahren (2015)	1.6‰	Kohn (2010)
$\delta^{13}C_{org(t)}$	Variable[a]	Diefendorf et al. (2015)[a]	Variable[a]	Diefendorf et al. (2015)[a]
A	28.26[b]	Schubert and Jahren (2012, 2013, 2015)	0[b]	Schubert and Jahren (2012, 2013, 2015)
B	0.22	This study	0.028	Bootstrapping (this study)
C	Median value determined in Monte Carlo analysis[c]	This study	Determined in Monte Carlo analysis[c]	This study

[a] Dataset used for calculation of $pCO_{2(t)}$ within Fig. 4 is provided in the Appendix.
[b] The value for A was fixed at 28.26.
[c] Calculated by solving Eq. (2) with $pCO_2 = 0$ and $\Delta^{13}C = 4.4$, such that $C = [4.4 \times (A)]/[(A - 4.4) \times (B)]$.

increases with increasing $pCO_{2(t)}$ and the positive error is higher than negative error (Fig. 3). The positive error reaches ~187% (~3730 ppmv) at $pCO_{2(t)} = \sim2000$ ppmv, but the negative error remains <~50% (~930 ppmv) across the entire range of $pCO_{2(t)}$ tested (Fig. 3). The calculated uncertainty (+122%/−40%) when the reconstructed $pCO_{2(t)}$ is below 1000 ppmv suggests that the C_3 plant proxy can be widely used across most of the Cenozoic, which is characterized by $pCO_2 \leqslant \sim1000$ ppmv (e.g., Pearson et al., 2009; Breecker et al., 2010; Beerling and Royer, 2011; Zhang et al., 2013; Franks et al., 2014). During brief carbon isotope excursion events when pCO_2 may exceed 2000 ppmv (e.g., Cui et al., 2011; Kiehl and Shields, 2013; Schubert and Jahren, 2013; Meissner et al., 2014), the relatively small negative error may be used to produce a minimum bound on the pCO_2 level reached.

Fig. 3 (bottom) shows that the 10,000 Monte Carlo resampling process generated a limited number of invalid $pCO_{2(t)}$ values (i.e., $pCO_{2(t)} < 0$ or $>10^6$ ppmv). The percentage of invalid $pCO_{2(t)}$ values reached a maximum of 28% at $pCO_{2(t)}$ close to 2000 ppmv, but accounted for <~5% of all values for $pCO_{2(t)} < \sim1000$ ppmv, and <1% of values were invalid for $pCO_{2(t)} < 400$ ppmv. These invalid numbers are a result of the hyperbolic relationship used, such that if $\Delta(\Delta^{13}C)$ exceeded 8.6‰ (assuming $pCO_{2(t=0)} = 270$ ppmv), calculated $pCO_{2(t)}$ will jump from infinitely high values (i.e., $\gg10^6$ ppmv) to the symmetrical branch of the hyperbola, and thus yield infinitely low $pCO_{2(t)}$ (i.e., $\ll0$ ppmv) (Supplementary Fig. 2). Because these negative $pCO_{2(t)}$ values resulted from exceedingly high $\Delta(\Delta^{13}C)$, and therefore do not indicate very low $pCO_{2(t)}$, these invalid $pCO_{2(t)}$ values (which can approach negative infinity) were removed. This is in contrast to an error analysis for the paleosol carbonate CO_2 paleobarometer, which replaces negative values with zeros (Breecker, 2013); for these paleosols, negative pCO_2 resulted from estimates that were slightly too low, rather than being exceedingly high.

Because of the nonlinear nature of the curve fitting function (Fig. 1), we expected the errors we quantified here to cause the median $pCO_{2(t)}$ determined *via* Monte Carlo resampling to be higher than if $pCO_{2(t)}$ were calculated simply using Eq. (7) (i.e., with no errors). However, for $pCO_{2(t)} > \sim1000$ ppmv, removal of the increasing number of invalid values (i.e., $pCO_{2(t)} < 0$ or $> 10^6$) generated during the Monte Carlo resampling caused a decrease in the median $pCO_{2(t)}$ value. Although $pCO_{2(t)} < 0$ or $>10^6$ can be calculated as a result of the hyperbolic function used (Supplementary Fig. 3), we conclude that the effect of these invalid values on reconstructed $pCO_{2(t)}$ is small at $pCO_{2(t)} < \sim1000$ ppmv, and well within the errors quantified here.

3.3. Application to the Paleogene

We reconstruct atmospheric pCO_2 from 63 to 52 Ma using uncertainties listed in Table 2 and the $\delta^{13}C_{org}$ dataset presented in Diefendorf et al. (2015) (Fig. 4). The reconstructed Paleogene pCO_2 levels based on 75 data points average 470 +288/−147 ppmv, and are consistent with other proxy estimates for this time period (Table 3). The calculated $pCO_{2(t)}$ estimates assume $\delta^{13}C_{org(t=0)} = -25.1$‰ at 270 ppmv (Holocene average pCO_2 and $\delta^{13}C_{org}$) (Table 2). Uncertainty in $\delta^{13}C_{org(t=0)}$ is estimated as ±1.6‰, which represents the standard deviation of 479 $\delta^{13}C$ measurements made on a wide diversity of modern leaves collected across ~55°S to 70°N latitude, and includes sites with MAP = ~1–3700 mm/yr (Kohn, 2010). We acknowledge, however, that inclusion of independent data on MAP could be used to better constrain the value for $\delta^{13}C_{org(t=0)}$ within this range (i.e., 1σ range = −26.7‰ to −23.5‰), with wetter and drier sites approximating values near the lower and higher ends of this range, respectively. However, by using the global uncertainty value of ±1.6‰ observed in leaves today, our analysis makes no attempt to include climate information in order to constrain the value for $\delta^{13}C_{org(t=0)}$ further. As a result, the errors in pCO_2 calculated here reflect conservative estimates, and provide opportunity for decreasing the errors in $pCO_{2(t)}$ provided that the paleoenvironment in which the plants grew can be constrained.

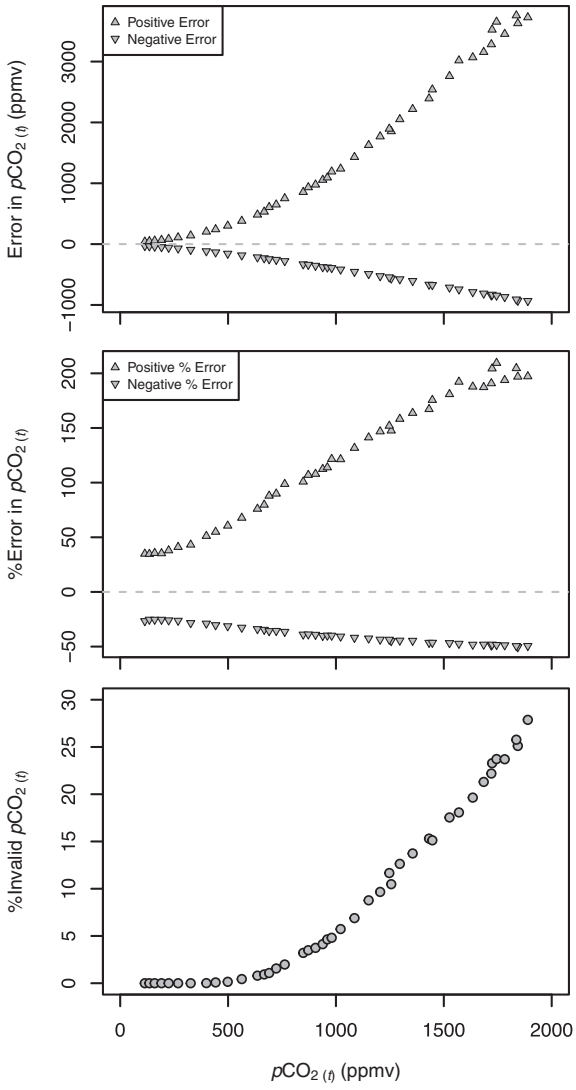

Fig. 3. Full error propagation showing the effect of all the uncertainties for the inputs listed in Table 2 on the error in $pCO_{2\,(t)}$. Top: the positive and negative $pCO_{2(t)}$ error in ppmv; middle: the positive and negative $pCO_{2(t)}$ error in percentage; bottom: the percent of invalid $pCO_{2(t)}$ values (i.e., $0 > pCO_{2(t)} > 10^6$ ppmv) generated during the 10,000 Monte Carlo resampling.

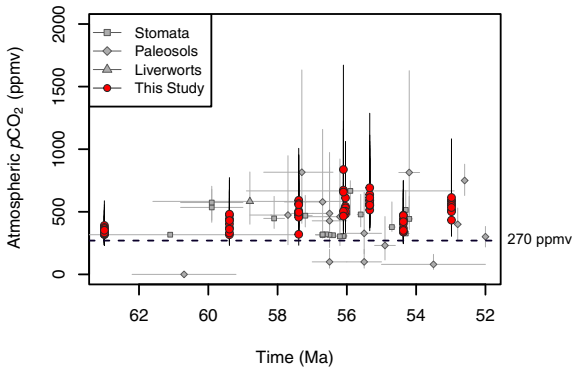

Fig. 4. Reconstruction of $pCO_{2(t)}$ (red circles with black error bars) for the Paleogene (52–63 Ma) using the C_3 land plant proxy and $\delta^{13}C_{org(t)}$ data from Diefendorf et al. (2015). All inputs and their uncertainties for calculation of $pCO_{2(t)}$ are listed in Table 2. The error bars on each calculated $pCO_{2(t)}$ value assume a lack of knowledge of the paleoenvironment of the site (i.e., use 1σ uncertainty of 1.6‰ based on a global dataset of modern leaf $\delta^{13}C_{org}$ values; Kohn, 2010). Note that the variability in reconstructed $pCO_{2(t)}$ for each time interval is small relative to the error bars, consistent with little variability in $\delta^{13}C_{org(t)}$ within each time interval. pCO_2 reconstructions based on the data compilation of Royer (2014) for three other proxies (gray symbols and error bars: squares, stomata; diamonds, paleosols; triangles, liverworts) are shown for comparison. $pCO_{2(t)}$ calculated using the C_3 land plant proxy indicates levels above the pre-industrial value of 270 ppmv (dashed line). Average $pCO_{2(t)}$ data for each proxy within this time interval are presented in Table 3. (For interpretation of the references to color in this figure legend, the reader is referred to the web version of this article.)

4. SENSITIVITY ANALYSIS OF INPUT ERRORS

Because this proxy analyzes the relative change in $\Delta^{13}C$ in response to a change in pCO_2, quantifying $pCO_{2(t)}$ requires knowledge of $\delta^{13}C_{CO2}$, $\delta^{13}C_{org}$, and pCO_2 for an initial time period ($t = 0$), as well as data on $\delta^{13}C_{org}$ and $\delta^{13}C_{CO2}$ at the time period of interest (t). Here we describe how uncertainty in these five input parameters, each in isolation, affects the error in $pCO_{2(t)}$ across $pCO_{2(t)} = \sim 110$ to ~ 2000 ppmv.

4.1. Sensitivity analysis of $pCO_{2(t=0)}$

The errors in $pCO_{2(t=0)}$ depend on the reference time period used. Modern measurements of pCO_2 have extremely low error from direct measurement of air (Keeling et al., 2009), but these are limited to only the most recent $\sim$50 years; ice core records extend back 800,000 years while maintaining low error (e.g., Holocene error = ±7 ppmv, Kawamura et al., 2007); and various proxies can extend the record back millions of years, but have significantly higher error (e.g., Neogene error is as low as ~35 ppmv for the alkenone and boron proxies; Royer, 2014). Because the error in pCO_2 is negligible when measured directly from today's atmosphere, we focus on comparison of the error in $pCO_{2(t)}$ that results when using $pCO_{2(t=0)}$ data from ice cores (±7 ppmv) *versus* Neogene proxy data (±35 ppmv), as our low and high uncertainty scenarios (Fig. 5). For both scenarios we set $pCO_{2(t=0)} = 270$ ppmv (pre-industrial value), but note that this is also similar to the median Neogene value determined from other proxies (i.e., ~314 ppmv; Royer, 2014). Because the error in $pCO_{2(t)}$ is a function of $pCO_{2(t=0)}$, our use of a low pCO_2 period for $t = 0$ results in greater error in $pCO_{2(t)}$ than if a reference period with higher pCO_2 were chosen, especially for when investigating periods with high $pCO_{2(t)}$.

As expected, the high $pCO_{2(t=0)}$ error scenario (i.e., ±35 ppmv) yielded more error on $pCO_{2(t)}$ than the low $pCO_{2(t=0)}$ error scenario (i.e., ±7 ppmv) across all $pCO_{2(t)}$ values (Fig. 5). Errors in $pCO_{2(t)}$ increased with increasing $pCO_{2(t)}$; however, the error in $pCO_{2(t)}$ increased at a faster rate for the ±35 ppmv scenario than the ±7 ppmv scenario, especially for the positive error (Fig. 5). For $pCO_{2(t)} > 270$ ppmv, the positive error is greater than the

Table 3
pCO_2 estimates and their reported errors (Royer, 2014) for the Paleogene (52–63 Ma) compared with calculated values for the C_3 plant proxy.

Paleogene					
Proxy	Age range (Ma)	Mean pCO_2 (ppmv)	Mean negative error in ppmv (%)	Mean positive error in ppmv (%)	No. of pCO_2 estimates
C_3 plant proxy (this study)	52–63	470	−147 (31%)[a]	288 (61%)[a]	75
Liverworts	58.8	583	−182 (31%)	235 (40%)	1
Paleosols	52–63	397	−173 (44%)	327 (82%)	16
Stomata	52–63	400	−54 (14%)	79 (20%)	22

[a] Determined from the Monte Carlo resampling (Fig. 4).

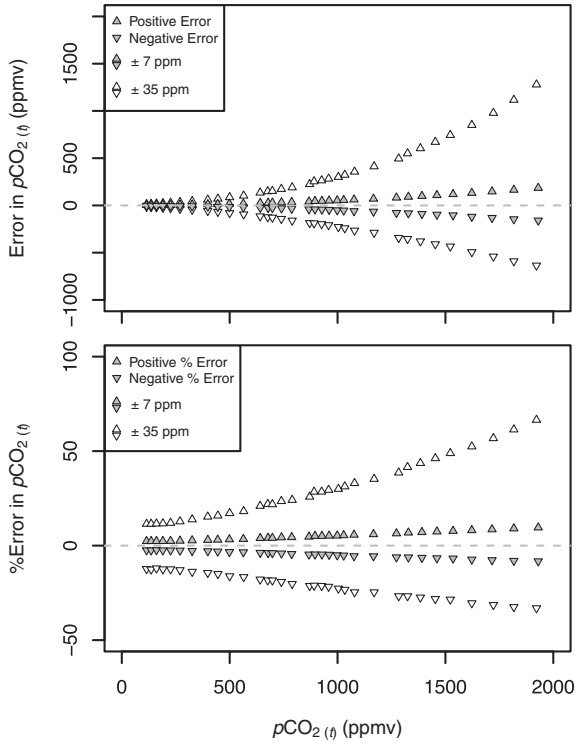

Fig. 5. Sensitivity analysis showing the effect of uncertainty in $pCO_{2(t=0)}$ on the errors in $pCO_{2(t)}$. Errors in $pCO_{2(t)}$ are shown for $pCO_{2(t=0)} = 270 \pm 7$ ppmv ($t = 0$, Holocene, shaded triangles) and $pCO_{2(t=0)} = 270 \pm 35$ ppmv ($t = 0$, Neogene, open triangles); all other input uncertainties are kept at 0. Top: $pCO_{2(t)}$ error in ppmv; bottom: $pCO_{2(t)}$ error in percentage.

negative error, consistent with expectations based on the curved shape of proxy relationship, but this offset is minimal (i.e., <3%) for the ±7 ppmv error scenario. The error in $pCO_{2(t)}$ associated with the curve fitting (Fig. 2) is in general higher than the error in $pCO_{2(t)}$ determined for the ±7 ppmv scenario, but lower than that determined using the ±35 ppmv scenario (Fig. 5). This result demonstrates the importance of minimizing the error in $pCO_{2(t=0)}$, especially if $pCO_{2(t)}$ is expected to be high.

4.2. Sensitivity analysis of $\delta^{13}C_{CO2}$

Here, we assessed how the uncertainty in the $\delta^{13}C_{CO2}$ value used to calculate $\Delta(\Delta^{13}C)$ (Eq. (5)) affected the error in $pCO_{2(t)}$ for two scenarios: ±0.1‰ and ±0.5‰. An uncertainty of ±0.1‰ corresponds with the uncertainty in $\delta^{13}C_{CO2}$ value from ice core records for the Holocene (Schmitt et al., 2012); an uncertainty of ±0.5‰ corresponds to the uncertainty reported for the Cenozoic from a reconstruction based on benthic foraminifera (Tipple et al., 2010). Error in $\delta^{13}C_{CO2}$ of ±0.2‰ assumed by Breecker and Retallack (2014) for the paleosol carbonate pCO_2 proxy falls within this range. We show the error analysis for $\delta^{13}C_{CO2(t)}$ specifically, but note that the error in $pCO_{2(t)}$ is nearly identical (<0.4% difference across all $pCO_{2(t)}$) whether these errors are applied to $\delta^{13}C_{CO2(t=0)}$ or $\delta^{13}C_{CO2(t)}$. For both scenarios, error increases with increasing $pCO_{2(t)}$, both in terms of absolute values (i.e., ppmv) and percent error (Fig. 6), similar to what we observed with the error in curve fitting (Fig. 2) and error in $pCO_{2(t=0)}$ (Fig. 5). The positive and negative errors in $pCO_{2(t)}$ are similar to each other when using an uncertainty of ±0.1‰, but for uncertainty of ±0.5‰ the positive error is significantly higher than the negative error, especially at high $pCO_{2(t)}$ (Fig. 6). The ±0.1‰ scenario yields smaller $pCO_{2(t)}$ error than the $pCO_{2(t=0)}$ uncertainty of ±7 ppmv scenario, while the ±0.5‰ scenario yields slightly smaller error than the ±35 ppmv scenario.

4.3. Sensitivity analysis of $\delta^{13}C_{org}$

A vast amount of $\delta^{13}C_{org}$ measurements have been produced from terrestrial plant tissue including bulk organic matter (e.g., Matson et al., 2012), wood (e.g., Treydte et al., 2007; Young et al., 2012), leaves (e.g., Graham et al., 2014), and leaf waxes (e.g., *n*-alkanes) (e.g., Rieley et al., 1991; Collister et al., 1994). Measurement error for $\delta^{13}C_{org}$ is almost always better than 0.2‰ and commonly better than 0.1‰ (e.g., Werner et al., 1999; King et al., 2012) and an error of ±0.12‰ for soil $\delta^{13}C_{org}$ was used in a recent analysis of the uncertainty in the paleosol carbonate pCO_2 proxy (Breecker, 2013). We note that significant changes in the measured $\delta^{13}C_{org}$ value can also result from changes in precipitation (e.g., Stewart et al., 1995; Kohn, 2010), plant communities (e.g., O'Leary, 1988; Flanagan et al., 1997), pO_2 (e.g., Berner et al., 2000; Beerling et al., 2002; Tappert et al., 2013), and source inputs (e.g., Walsh et al., 2008; Rebolledo et al., 2015), and thus can affect the accuracy of the reconstructed pCO_2 value. Similar effects are commonly resolved in other pCO_2 proxies by producing multiple reconstructed pCO_2 values

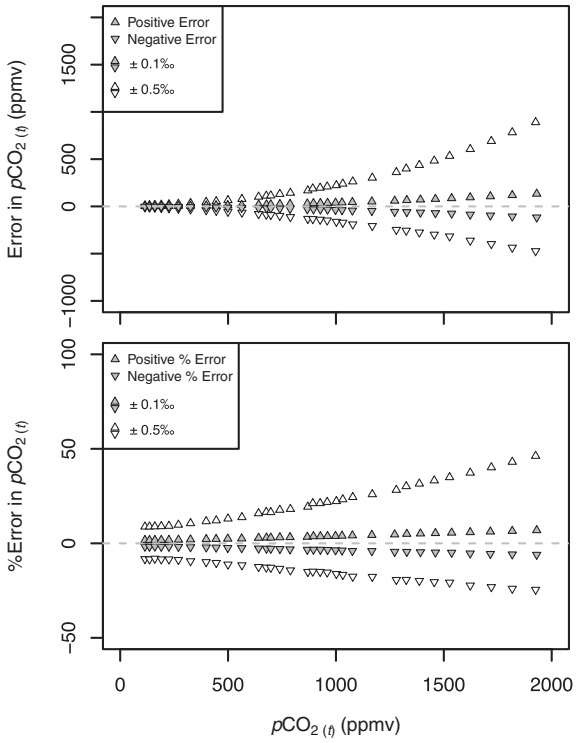

Fig. 6. Sensitivity analysis showing the effect of uncertainty in $\delta^{13}C_{CO2}$ on the errors in $pCO_{2(t)}$. Errors in $pCO_{2(t)}$ are shown for $\delta^{13}C_{CO2(t)} = \pm 0.1‰$ (shaded triangles) and $\delta^{13}C_{CO2(t)} = \pm 0.5‰$ (open triangles); all other input uncertainty is kept at 0. The error in $pCO_{2(t)}$ is applied here to the $\delta^{13}C_{CO2(t)}$ term within Eq. (7), but is nearly identical (<~0.4% difference across all $pCO_{2(t)}$) whether this error is applied to $\delta^{13}C_{CO2(t=0)}$ or $\delta^{13}C_{CO2(t)}$. Top: $pCO_{2(t)}$ error in ppmv; bottom: $pCO_{2(t)}$ error in percentage.

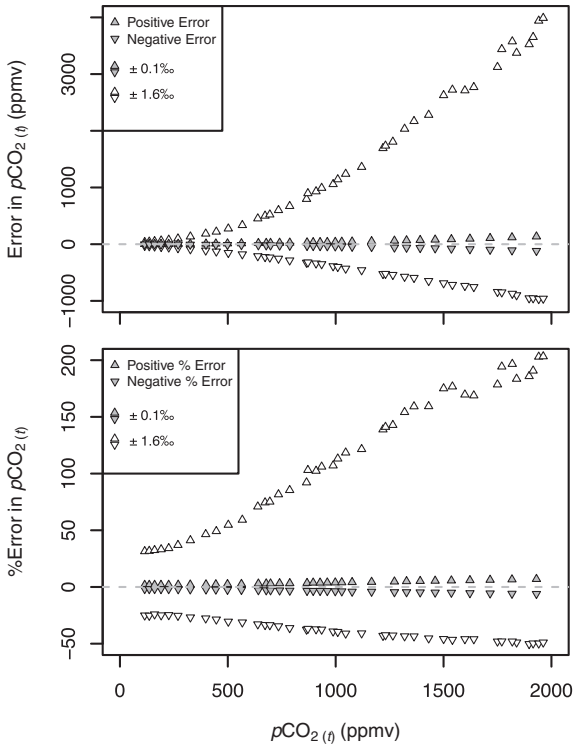

Fig. 7. Sensitivity analysis showing the effect of uncertainty in $\delta^{13}C_{org}$ on the errors in $pCO_{2(t)}$. Errors in $pCO_{2(t)}$ are shown for $\delta^{13}C_{org(t=0)}=\pm 0.1‰$ (shaded triangles) and $\delta^{13}C_{org(t=0)}=\pm 1.6‰$ (open triangles); all other input uncertainty is kept at 0. The error in $pCO_{2(t)}$ is applied here to the $\delta^{13}C_{org(t\,=\,0)}$ term within Eq. (7), but is nearly identical (<~0.4% difference across all $pCO_{2(t)}$) whether this error is applied to $\delta^{13}C_{org(t=0)}$ or $\delta^{13}C_{org(t)}$. Top: $pCO_{2\,(t)}$ error in ppmv; bottom: $pCO_{2(t)}$ error in percentage.

for a given time period, with each reconstructed pCO_2 value having its own uncertainty (e.g., Cleveland et al., 2008; Steinthorsdottir et al., 2011; Royer et al., 2014; Whiteside et al., 2015). By producing a large number of values, consensus in the pCO_2 value may be achieved (Beerling and Royer, 2011), but the accuracy of such a proxy value is impossible to verify for deep time applications. Instead, workers often assess the accuracy of the proxies by comparison with available ice core or modern pCO_2 data (e.g., Tripati et al., 2009; Franks et al., 2014; Schubert and Jahren, 2015).

Leaves from modern C_3 plants growing in equilibrium with a well-mixed atmosphere show a large range of $\delta^{13}C_{org}$ values (−31.2‰ to −22.8‰, $n = 479$, Kohn, 2010). The standard deviation of this global dataset is $\pm$ 1.6‰ and represents a good estimate of the $\pm 1\sigma$ uncertainty of $\delta^{13}C_{org(t=0)}$. A similar approach was used in a recent error quantification study on hydrogen isotopes by Polissar and D'Andrea (2014). Use of this uncertainty value assumes that the Holocene experienced similar variability in $\delta^{13}C_{org}$ as modern plants and no information on plant type or climate is known for the site. Here we present a sensitivity analysis in $\delta^{13}C_{org(t=0)}$ by comparing two end-member scenarios for the uncertainty in $pCO_{2(t)}$: natural, environmental variability across diverse environments and plant types (i.e., ±1.6‰) and uncertainty only associated with measurement error (i.e., ±0.1‰). For both scenarios, error increases with increasing $pCO_{2(t)}$, both in terms of absolute values (i.e., ppmv) and percent error, but the higher uncertainty scenario (i.e., ±1.6‰) results in a much faster increase in uncertainty of $pCO_{2(t)}$ (Fig. 7). The positive and negative errors in $pCO_{2(t)}$ are similar to each other when using an uncertainty of ±0.1‰, but for uncertainty of ±1.6‰ the positive error is >3 times higher than the negative error, especially at high $pCO_{2(t)}$ (Fig. 7). This illustrates that without independent knowledge of environmental conditions at the site, uncertainty in $\delta^{13}C_{org(t=0)}$ produces the largest error in $pCO_{2(t)}$ of any of the input parameters. This suggests that improvement in the estimate of $\delta^{13}C_{org(t=0)}$ is a useful target for reducing the uncertainty in this proxy.

5. COMPARISON WITH OTHER PROXIES

We compare the error of our C_3 land plant pCO_2 proxy to the errors of other proxies (e.g., fossil leaf stomatal indices, boron isotopes, paleosol carbonates, liverworts, alkenones, and stomatal ratio) across a wide range of pCO_2 (Fig. 8). The positive error of the C_3 plant proxy increases at a somewhat faster rate with increasing pCO_2

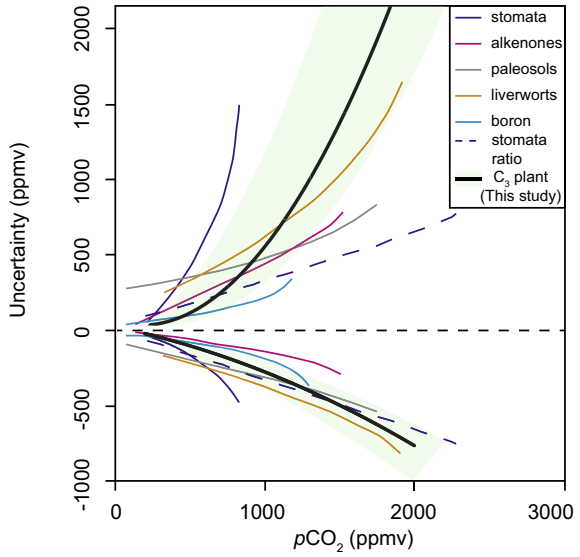

Fig. 8. Positive and negative errors of pCO_2 proxies redrawn from Fig. 3 within Royer (2014) plotted with the errors of the C_3 land plant proxy from this study. Errors in $pCO_{2(t)}$ are calculated using the uncertainties shown in Table 2, but with error for $\delta^{13}C_{org(t=0)}$ ranging from ±0.1‰ (measurement error) to ±1.6‰ (environmental error) (shaded region). Bold black line represents a second order polynomial fit through the error data if the $\delta^{13}C_{org(t=0)}$ error is reduced to ±0.7‰.

than most other proxies at very high pCO_2, and is comparable to the liverworts-based proxy at $pCO_2 =$ ~1000 ppmv). The negative error of the C_3 plant proxy increases more slowly with increasing pCO_2 and follows general trends observed in the other pCO_2 proxies. If one can independently constrain the plant functional type or the climate, the error on $pCO_{2(t)}$ can be reduced significantly (Fig. 8).

The right-skewed error of the C_3 plant proxy is similar to that observed for liverworts (Fletcher et al., 2008), stomata (Beerling et al., 2009) and paleosols (Royer 2014). Unlike the paleosol carbonate pCO_2 proxy, for which the right skewed error can be minimized by choosing evenly balanced soil CO_2 mixtures (Breecker, 2013), the right skew to the error in pCO_2 is inherent to the C_3 plant pCO_2 proxy because of the nonlinear curve fitting function.

Typically, high-resolution pCO_2 reconstructions are limited to marine substrates. However, recent application of the C_3 land plant proxy towards reconstructing pCO_2 across the last 30 kyr (Schubert and Jahren, 2015) demonstrated the potential for generating nearly continuous records of pCO_2 from terrestrial environments. The relatively low error determined here for this proxy (e.g., Fig. 4), especially at low to moderate pCO_2, combined with the large abundance of terrestrial organic matter throughout the fossil record, suggests great potential for generating similar high-resolution pCO_2 records across millions of years of Earth history. Comparison of high-resolution terrestrial and marine pCO_2 records would help to validate these reconstructions and provide necessary data for comparing to available high-resolution temperature records (e.g., high-resolution oxygen isotope records, Zachos et al., 2001). The application of statistically robust uncertainty analyses to these reconstructions can improve our understanding of uncertainty when evaluating Earth system climate sensitivity (e.g., Royer et al., 2007).

6. IMPLICATIONS AND CONCLUSION

This study provides a rigorous statistical analysis of the error in the C_3 land plant pCO_2 proxy using a Monte Carlo resampling method. The errors in $pCO_{2(t)}$ increase with increasing $pCO_{2(t)}$ and the positive errors are generally at least as high as the negative errors for all scenarios (Fig. 3), similar to several other pCO_2 proxies (Fig. 8). The percent errors we estimate for $pCO_{2(t)}$ during the Paleogene (+61%/−31%) are within the range of errors determined from the other pCO_2 proxies (+20% to +82% and −14% to −44%) (Table 3). For time periods with large changes in pO_2 (e.g., the late Paleozoic, Berner, 2006), we acknowledge the need to better quantify the effect of pO_2 on $\Delta^{13}C$ in plants grown from seed to maturity across multiple levels of pO_2 spanning this range. In addition, we point to better determination of the paleoenvironment of a site as an opportunity to reduce the errors in $pCO_{2(t)}$ presented here. Last, although calculated $pCO_{2(t)}$ values show little variability within each time interval examined here (Fig. 4), we acknowledge that use of large $\delta^{13}C_{org(t)}$ datasets is desirable. For example, a recent analysis determined that by averaging 50 randomly selected paleosols within each time slice, one could significantly reduce the uncertainty in paleosols-based pCO_2 estimates (Breecker, 2013). The increasing availability of terrestrial $\delta^{13}C$ measurements from fossil organic matter, leaves, and specific compounds (e.g., leaf waxes, cellulose) and the relatively low errors for this proxy across a wide range of pCO_2 suggests great potential for applying this proxy throughout much of the fossil record of C_3 land plants, when pCO_2 may have remained <1000 ppmv (Franks et al., 2014).

ACKNOWLEDGEMENTS

This research was supported by the Chemical Sciences, Geosciences and Biosciences Division, Office of Basic Energy Sciences, Office of Science, U.S. Department of Energy under award DE-FG02-13ER16412 to B.A.S.

APPENDIX A. SUPPLEMENTARY DATA

Supplementary data associated with this article can be found, in the online version, at http://dx.doi.org/10.1016/j.gca.2015.09.032.

REFERENCES

Beerling D. J. and Royer D. L. (2011) Convergent Cenozoic CO_2 history. *Nat. Geosci.* **4**(7), 418–420.

Beerling D. J., Lake J. A., Berner R. A., Hickey L. J., Taylor D. W. and Royer D. L. (2002) Carbon isotope evidence implying high O_2/CO_2 ratios in the Permo-Carboniferous atmosphere. *Geochim. Cosmochim. Acta* **66**, 3757–3767.

Beerling D. J., Fox A. and Anderson C. W. (2009) Quantitative uncertainty analyses of ancient atmospheric CO_2 estimates from fossil leaves. *Am. J. Sci.* **309**(9), 775–787.

Berner R. A. (2006) GEOCARBSULF: A combined model for Phanerozoic atmospheric O_2 and CO_2. *Geochim. Cosmochim. Acta* **70**, 5653–5664.

Berner R. A., Petsch S., Lake J., Beerling D., Popp B., Lane R., Laws E., Westley M., Cassar N. and Woodward F. (2000) Isotope fractionation and atmospheric oxygen: Implications for Phanerozoic O_2 evolution. *Science* **287**, 1630–1633.

Bonal D., Sabatier D., Montpied P., Tremeaux D. and Guehl J. (2000) Interspecific variability of $\delta^{13}C$ among trees in rainforests of French Guiana: functional groups and canopy integration. *Oecologia* **124**, 454–468.

Breecker D. (2013) Quantifying and understanding the uncertainty of atmospheric CO_2 concentrations determined from calcic paleosols. *Geochem. Geophys. Geosyst.* **14**(8), 3210–3220.

Breecker D. O. and Retallack G. J. (2014) Refining the pedogenic carbonate atmospheric CO_2 proxy and application to Miocene CO_2: *Palaeogeography. Palaeoclimatology, Palaeoecology* **406**, 1–8.

Breecker D. O., Sharp Z. D. and McFadden L. D. (2010) Atmospheric CO_2 concentration during ancient greenhouse climates were similar to those predicted for A.D. 2100. *Proc. Natl. Acad. Sci. U.S.A.* **107**(2), 576–580.

Cerling T. (1991) Carbon dioxide in the atmosphere: evidence from Cenozoic and Mesozoic paleosols. *Am. J. Sci.* **291**(4), 377–400.

Cerling T. E., Solomon D. K., Quade J. and Bowman J. R. (1991) On the isotopic composition of carbon in soil carbon dioxide. *Geochim. Cosmochim. Acta* **55**(11), 3403–3405.

Christeller J. T., Laing W. A. and Troughton J. H. (1976) Isotope discrimination by ribulose 1, 5-diphosphate carboxylase: no effect of temperature or HCO_3^- concentration. *Plant Physiol.* **57** (4), 580–582.

Cleveland D. M., Nordt L. C., Dworkin S. I. and Atchley S. C. (2008) Pedogenic carbonate isotopes as evidence for extreme climatic events preceding the Triassic–Jurassic boundary: implications for the biotic crisis? *Geol. Soc. Am. Bull.* **120**(11–12), 1408–1415.

Collister J. W., Rieley G., Stern B., Eglinton G. and Fry B. (1994) Compound-specific $\delta^{13}C$ analyses of leaf lipids from plants with differing carbon dioxide metabolisms. *Org. Geochem.* **21**(6–7), 619–627.

Craig H. (1953) The geochemistry of the stable carbon isotopes. *Geochim. Cosmochim. Acta* **3**(2), 53–92.

Cui Y., Kump L. R., Ridgwell A. J., Charles A. J., Junium C. K., Diefendorf A. F., Freeman K. H., Urban N. M. and Harding I. C. (2011) Slow release of fossil carbon during the Palaeocene-Eocene Thermal Maximum. *Nat. Geosci.* **4**(7), 481–485.

Demicco R. V., Lowenstein T. K. and Hardie L. A. (2003) Atmospheric pCO_2 since 60 Ma from records of seawater pH, calcium, and primary carbonate mineralogy. *Geology* **31**(9), 793–796.

Diefendorf A. F., Mueller K. E., Wing S. L., Koch P. L. and Freeman K. H. (2010) Global patterns in leaf ^{13}C discrimination and implications for studies of past and future climate. *Proc. Natl. Acad. Sci.* **107**(13), 5738–5743.

Diefendorf A. F., Freeman K. H., Wing S. L., Currano E. D. and Mueller K. E. (2015) Paleogene plants fractionated carbon isotopes similar to modern plants. *Earth Planet. Sci. Lett.* **429**, 33–44.

Efron B. and Tibshirani R. J. (1994) *An Introduction to the Bootstrap*. CRC Press.

Ekart D. D., Cerling T. E., Montanez I. P. and Tabor N. J. (1999) A 400 million year carbon isotope record of pedogenic carbonate: implications for paleoatmospheric carbon dioxide. *Am. J. Sci.* **299**(10), 805–827.

Farquhar G. D., O'Leary M. H. and Berry J. A. (1982) On the relationship between carbon isotope discrimination and the intercellular carbon dioxide concentration in leaves. *Aust. J. Plant Physiol.* **9**, 121–137.

Farquhar G., Ehleringer J. and Hubick K. (1989) Carbon isotope discrimination and photosynthesis. *Annu. Rev. Plant Biol.* **40**, 503–537.

Flanagan L. B., Brooks J. R. and Ehleringer J. R. (1997) Photosynthesis and carbon isotope discrimination in boreal forest ecosystems: a comparison of functional characteristics in plants from three mature forest types. *J. Geophys. Res. Atmos. (1984–2012)* **102**(D24), 28861–28869.

Fletcher B. J., Beerling D. J., Brentnall S. J. and Royer D. L. (2005) Fossil bryophytes as recorders of ancient CO_2 levels: experimental evidence and a Cretaceous case study. *Global Biogeochem. Cycles* **19**(3).

Fletcher B. J., Brentnall S. J., Quick W. P. and Beerling D. J. (2006) BRYOCARB: a process-based model of thallose liverwort carbon isotope fractionation in response to CO_2, O_2, light and temperature. *Geochim. Cosmochim. Acta* **70**(23), 5676–5691.

Fletcher B. J., Brentnall S. J., Anderson C. W., Berner R. A. and Beerling D. J. (2008) Atmospheric carbon dioxide linked with Mesozoic and early Cenozoic climate change. *Nat. Geosci.* **1**(1), 43–48.

Franks P. J., Royer D. L., Beerling D. J., Van de Water P. K., Cantrill D. J., Barbour M. M. and Berry J. A. (2014) New constraints on atmospheric CO_2 concentration for the Phanerozoic. *Geophys. Res. Lett.*, 2014GL060457.

Freeman K. H. and Pagani M. (2005) Alkenone-based estimates of past CO_2 levels: a consideration of their utility based on an analysis of uncertainties. In *A History of Atmospheric CO2 and Its Effects on Plants, Animals, and Ecosystems* (eds. J. Ehleringer, T. Cerling and D. Dearing). American Geophysical Union, pp. 55–78.

Graham H. V., Patzkowsky M. E., Wing S. L., Parker G. G., Fogel M. L. and Freeman K. H. (2014) Isotopic characteristics of canopies in simulated leaf assemblages. *Geochim. Cosmochim. Acta* **144**, 82–95.

Guy R. D., Fogel M. L. and Berry J. A. (1993) Photosynthetic fractionation of the stable isotopes of oxygen and carbon. *Plant Physiol.* **101**, 37–47.

Hoins M., Van de Waal D. B., Eberlein T., Reichart G.-J., Rost B. and Sluijs A. (2015) Stable carbon isotope fractionation of organic cyst-forming dinoflagellates: evaluating the potential for a CO_2 proxy. *Geochim. Cosmochim. Acta* **160**, 267–276.

Jahren A. H. (2004) The carbon stable isotope composition of pollen. *Rev. Palaeobot. Palynol.* **132**, 291–313.

Kanzaki Y. and Murakami T. (2015) Estimates of atmospheric CO_2 in the Neoarchean-Paleoproterozoic from paleosols. *Geochim. Cosmochim. Acta* **159**, 190–219.

Kawamura, K., Nakazawa, T., Aoki, S., Sugawara, S., Fujii, Y. and Watanabe, O. (2007) Dome Fuji Ice Core 338KYr Wet Extraction CO_2 Data, in World Data Center for Paleoclimatology, Boulder and NOAA Paleoclimatology Program.

Keeling, R. F., Piper, S. C., Bollenbacher, A. F. and Walker, J. S. (2009) Atmospheric CO_2 records from sites in the SIO air sampling network. In Trends: A Compendium of Data on Global Change. Carbon Dioxide Information Analysis Center, Oak Ridge National Laboratory, U.S. Department of Energy, Oak Ridge, TN, U.S.A. doi: http://dx.doi.org/10.3334/CDIAC/atg.035.

Kiehl J. T. and Shields C. A. (2013) Sensitivity of the Palaeocene-Eocene Thermal Maximum climate to cloud properties. *Philos. Trans. Roy. Soc. Math. Phys. Eng. Sci.* **371**(2001), 20130093.

King D. C., Schubert B. A. and Jahren A. H. (2012) Practical considerations for the use of pollen $\delta^{13}C$ value as a paleoclimate indicator. *Rapid Commun. Mass Spectrom.* **26**, 2165–2172.

Kohn M. J. (2010) Carbon isotope compositions of terrestrial C3 plants as indicators of (paleo)ecology and (paleo)climate. *Proc. Natl. Acad. Sci.* **107**(46), 19691–19695.

Konrad W., Roth-Nebelsick A. and Grein M. (2008) Modelling of stomatal density response to atmospheric CO_2. *J. Theor. Biol.* **253**, 638–658.

Leavitt S. and Newberry T. (1992) Systematics of stable-carbon isotopic differences between gymnosperm and angiosperm trees. *Plant Physiol.* **11**, 257–262.

Lloyd J. and Farquhar G. D. (1994) ^{13}C discrimination during CO_2 assimilation by the terrestrial biosphere. *Oecologia* **99**(3–4), 201–215.

Lowenstein T. K. and Demicco R. V. (2006) Elevated Eocene atmospheric CO_2 and its subsequent decline. *Science* **313**(5795), 1928.

Martínez-Botí M. A., Foster G. L., Chalk T. B., Rohling E. J. and Sexton P. F., et al. (2015) Plio-Pleistocene climate sensitivity evaluated using high-resolution CO_2 records. *Nature* **518**, 49–54.

Matson S. D., Rook L., Oms O. and Fox D. L. (2012) Carbon isotopic record of terrestrial ecosystems spanning the Late Miocene extinction of *Oreopithecus bambolii*, Baccinello Basin (Tuscany, Italy). *J. Hum. Evol.* **63**(1), 127–139.

Meissner K., Bralower T., Alexander K., Jones T. D., Sijp W. and Ward M. (2014) The Paleocene-Eocene Thermal Maximum: how much carbon is enough? *Paleoceanography* **29**(10), 946–963.

O'Leary M. H. (1988) Carbon isotopes in photosynthesis. *BioScience* **38**, 328–336.

Pagani M., Arthur M. A. and Freeman K. H. (1999) Miocene evolution of atmospheric carbon dioxide. *Paleoceanography* **14**(3), 273–292.

Passey B. H., Cerling T. E., Perkins M. E., Voorhies M. R., Harris J. M. and Tucker S. T. (2002) Environmental change in the Great Plains: an isotopic record from fossil horses. *J. Geol.* **110**(2), 123–140.

Pearson P. N. and Palmer M. R. (2000) Atmospheric carbon dioxide concentrations over the past 60 million years. *Nature* **406**, 695–699.

Pearson P. N., Foster G. L. and Wade B. S. (2009) Atmospheric carbon dioxide through the Eocene–Oligocene climate transition. *Nature* **461**, 1110–1113.

Polissar P. J. and D'Andrea W. J. (2014) Uncertainty in paleohydrologic reconstructions from molecular δD values. *Geochim. Cosmochim. Acta* **129**, 146–156.

R Core Team (2015) *R: A Language and Environment for Statistical Computing*. R Foundation for Statistical Computing, Vienna, Austria, ISBN 3-900051-07-0, URL: http://www.R-project.org/.

Rebolledo, L., Lange, C. B., Bertrand, S., Muñoz, P., Salamanca, M., Lazo, P., Iriarte, J. L., Vargas, G., Pantoja, S. and Dezileau, L. (2015) Late Holocene precipitation variability recorded in the sediments of Reloncaví Fjord (41°S, 72°W), Chile: *Quaternary Research*, doi: http://dx.doi.org/10.1016/j.yqres.2015.05.006.

Rieley G., Collier R. J., Jones D. M., Eglinton G., Eakin P. A. and Fallick A. E. (1991) Sources of sedimentary lipids deduced from stable carbon-isotope analyses of individual compounds. *Nature* **352**, 425–427.

Roeske C. and O'Leary M. H. (1984) Carbon isotope effects on enzyme-catalyzed carboxylation of ribulose bisphosphate. *Biochemistry* **23**(25), 6275–6284.

Royer D. (2014) Atmospheric CO_2 and O_2 during the Phanerozoic: tools, patterns, and impacts. *Treatise Geochem.* **6**, 251–267.

Royer D. L., Berner R. A. and Beerling D. J. (2001) Phanerozoic atmospheric CO_2 change: evaluating geochemical and paleobiological approaches. *Earth Sci. Rev.* **54**(4), 349–392.

Royer D. L., Berner R. A. and Park J. (2007) Climate sensitivity constrained by CO_2 concentrations over the past 420 million years. *Nature* **446**(7135), 530–532.

Royer D. L., Donnadieu Y., Park J., Kowalczyk J. and Goddéris Y. (2014) Error analysis of CO_2 and O_2 estimates from the long-term geochemical model GEOCARBSULF. *Am. J. Sci.* **314**(9), 1259–1283.

Schmitt J., Schneider R., Elsig J., Leuenberger D., Lourantou A., Chappellaz J., Köhler P., Joos F., Stocker T. F. and Leuenberger M. (2012) Carbon isotope constraints on the deglacial CO_2 rise from ice cores. *Science* **336**(6082), 711–714.

Schubert B. A. and Jahren A. H. (2012) The effect of atmospheric CO_2 concentration on carbon isotope fractionation in C_3 land plants. *Geochim. Cosmochim. Acta* **96**, 29–43.

Schubert B. A. and Jahren A. H. (2013) Reconciliation of marine and terrestrial carbon isotope excursions based on changing atmospheric CO_2 levels. *Nat. Commun.* **4**, 1653. http://dx.doi.org/10.1038/ncomms2659.

Schubert B. A. and Jahren A. H. (2015) Global increase in plant carbon isotope fractionation following the Last Glacial Maximum caused by increase in atmospheric pCO_2. *Geology* **43**(5), 435–438.

Steinthorsdottir M., Jeram A. J. and McElwain J. C. (2011) Extremely elevated CO_2 concentrations at the Triassic/Jurassic boundary. *Palaeogeogr. Palaeoclimatol. Palaeoecol.* **308**, 418–432.

Stewart G. R., Turnbull M. H., Schmidt S. and Erskine P. D. (1995) ^{13}C natural abundance in plant communities along a rainfall gradient: a biological integrator of water availability. *Aust. J. Plant Physiol.* **22**, 51–55.

Strauss H. and Peters-Kottig W. (2003) The Paleozoic to Mesozoic carbon cycle revisited: the carbon isotopic composition of terrestrial organic matter. *Geochem. Geophys. Geosyst.* **4**(10).

Suits N. S., Denning A. S., Berry J. A., Still C. J., Kaduk J., Miller J. B. and Baker I. T. (2005) Simulation of carbon isotope discrimination of the terrestrial biosphere. *Global Biogeochem. Cycles* **19**, GB1017. http://dx.doi.org/10.1029/2003GB002141.

Tappert R., McKellar R. C., Wolfe A. P., Tappert M. C., Ortega-Blanco J. and Muehlenbachs K. (2013) Stable carbon isotopes of C3 plant resins and ambers record changes in atmospheric oxygen since the Triassic. *Geochim. Cosmochim. Acta* **121**, 240–262.

Tipple B. J., Meyers S. R. and Pagani M. (2010) Carbon isotope ratio of Cenozoic CO_2: a comparative evaluation of available geochemical proxies. *Paleoceanography* **25**, a, PA3202.

Treydte et al. (2007) Signal strength and climate calibration of a European tree-ring isotope network. *Geophys. Res. Lett.* **34**, L24302.

Tripati A. K., Roberts C. D. and Eagle R. A. (2009) Coupling of CO_2 and ice sheet stability over major climate transitions of the last 20 million years. *Science* **326**(5958), 1394–1397.

van de Wal R. S. W., de Boer B., Lourens L. J., Köhler P. and Bintanja R. (2011) Reconstruction of a continuous high-resolution CO_2 record over the past 20 million years. *Clim. Past* **7**, 1459–1469.

Walsh E. M., Ingalls A. E. and Keil R. G. (2008) Sources and transport of terrestrial organic matter in Vancouver Island fjords and the Vancouver-Washington Margin: A multiproxy approach using $\delta^{13}C_{org}$, lignin phenols, and the ether lipid BIT index. *Limnol. Oceanogr.* **53**(3), 1054–1063.

Werner R. A., Bruch B. A. and Brand W. A. (1999) ConFlo III—an interface for high precision $\delta^{13}C$ and $\delta^{15}N$ analysis with an extended dynamic range. *Rapid Commun. Mass Spectrom.* **13** (13), 1237–1241.

Whiteside J. H., Lindström S., Irmis R. B., Glasspool I. J., Schaller M. F., Dunlavey M., Nesbitt S. J., Smith N. D. and Turner A. H. (2015) Extreme ecosystem instability suppressed tropical dinosaur dominance for 30 million years. *Proc. Natl. Acad. Sci.* **112**(26), 7909–7913.

Wong W. W., Benedict C. R. and Kohel R. J. (1979) Enzymic fractionation of the stable carbon isotopes of carbon dioxide by ribulose-1,5-bisphosphate carboxylase. *Plant Physiol.* **63**(5), 852–856.

Wong C. I. and Breecker D. O. (2015) Advancements in the use of speleothems as climate archives. *Quaternary Sci. Rev.*. http://dx.doi.org/10.1016/j.quascirev.2015.07.019.

Ye Y. (1987) *Interior algorithms for linear, quadratic, and linearly constrained non linear programming* (PhD Dissertation). Stanford University.

Young G., McCarroll D., Loader N., Gagen M., Kirchhefer A. and Demmler J. (2012) Changes in atmospheric circulation and the Arctic Oscillation preserved within a millennial length reconstruction of summer cloud cover from northern Fennoscandia. *Clim. Dyn.* **39**(1), 495–507.

Zachos J. C., Pagani M., Sloan L., Thomas E. and Billups K. (2001) Trends, rhythms, and aberrations in global climate 65 Ma to present. *Science* **292**, 686–693.

Zhang Y. G., Pagani M., Liu Z., Bohaty S. M. and DeConto R. (2013) A 40-million-year history of atmospheric CO_2. *Philos. Trans. Roy. Soc. Math. Phys. Eng. Sci.* **371**(2001), 20130096.

Associate editor: Alex L. Sessions